Orientation Preference of Recrystallization in Supersaturated Aluminum Alloys Influenced by Concurrent Precipitation

QINGLONG ZHAO, KE HUANG, YANJUN LI, and KNUT MARTHINSEN

The influence of concurrent precipitation on recrystallization is analyzed by comparing the nucleation and growth behavior of P ($\{011\}$ $\langle566\rangle$), Cube ($\{001\}$ $\langle100\rangle$), and 20 deg ND-rotated Cube ($\{001\}$ $\langle310\rangle$, NDcube)-oriented grains in Al-xMn-Fe-Si ($x = 0$, 0.4, 1.0 wt pct) alloys. The number densities of recrystallized grains in alloys annealed at various temperatures clearly demonstrate that concurrent precipitation significantly reduces the nucleation density of recrystallization. However, this effect varies strongly with grain orientation, and the P orientation is affected less than other orientations, in particular the Cube orientation. The number fraction of P-oriented grains can increase ten times as the effect of concurrent precipitation enhances. The P- and NDcube-oriented grains grow faster than Cube grains when strong concurrent precipitation occurs. However, on the other hand, when precipitation is limited or completely absent, P grains grow more slowly than Cube (and NDcube) grains. Micro-segregation enhances the effect of concurrent precipitation, indicating that the effect is closely related to heterogeneous distribution of precipitation.

I. INTRODUCTION

THE control of grain size and texture is of important concern in aluminum sheet production, and recrystallization plays a vital part in the thermo-mechanical processing. Commercial aluminum usually contains second-phase particles formed during casting, and a large amount of alloying elements and impurities remain in solid solution, leading to precipitation during subsequent heat treatments. In supersaturated alloys, precipitation might occur during back annealing, which can interact with and strongly affect the recrystallization behavior. The recrystallization behavior of supersaturated alloys is divided into three regimes[1]: (I) precipitation prior to recrystallization; (II) precipitation and recrystallization occur concurrently; and III) recrystallization before precipitation. In regime I & II, a high density of fine precipitates induces a strong Zener drag effect, leading to slow recrystallization kinetics and coarse elongated grains.[2-7] By contrast, coarse particles can accelerate recrystallization by particle-stimulated

nucleation (PSN), for which recrystallization originates at subgrains in the deformation zones which develop around coarse particles at large strains.[8] Three-dimensional (3D) characterization in a particle-containing AA3104 alloy cold rolled to a reduction of 80 pct in thickness has shown that most of the nuclei are formed around clusters/bands of coarse particles.[9] The development of PSN in polycrystalline materials usually weakens the texture.[10,11] Nevertheless, in alloys containing coarse particles, it is often found in conditions of strong concurrent precipitation, strong P (typically $\{011\}$ $\langle566\rangle$) and ND-rotated cube ($\{001\}$ $\langle310\rangle$) texture components may develop during recrystallization.[3,5-7] Numerical simulations and electron back scattering diffraction (EBSD) observations have demonstrated that P orientations tend to form ahead of the coarse particle and that ND-rotated cube grains also originate within deformation zones.[12,13] It is suggested that these texture components are favored due to their low stored energy, which is indicated by Taylor factor.[14,15] It is further reported that the P-texture becomes more pronounced for low heating rates, compared to flash annealing, when precipitation occurs prior to or concurrently with recrystallization.[13] In a supersaturated Al-1.3 Mn alloy, it was found that precipitation occurred preferentially at high-angle boundaries,[2] which induces a stronger Zener drag effect than randomly distributed precipitates.[10,16] X-ray diffraction (XRD) and EBSD investigations of recrystallization textures in supersaturated Al-Mn-(Mg) alloys suggest that the intensity of the P-component increases with decreasing annealing temperature and/or increased rolling reduction.[17-19] In the work by Schäfer et al., it was documented that more P-oriented grains are generated

QINGLONG ZHAO, formerly Researcher with the Department of Materials Science and Engineering, Norwegian University of Science and Technology, 7491 Trondheim, Norway, is now Associate Professor with the Key Laboratory of Automobile Materials, Ministry of Education, and Department of Materials Science and Engineering, Jilin University, Changchun 130025, P.R. China. Contact e-mails: qinglong. zhao@gmail.com, zhaoqinglong@jlu.edu.cn KE HUANG, Scientist, is with Laboratory of Thermomechanical Metallurgy - PX Group Chair, Ecole Polytechnique Fédérale de Lausanne, Neuchâtel CH-2002, Switzerland. YANJUN LI and KNUT MARTHINSEN, Professors, are with Department of Materials Science and Engineering, Norwegian University of Science and Technology. Contact e-mail: knut.marthinsen@ntnu.no

Manuscript submitted June 13, 2015.
Article published online January 4, 2016.

at the large particles in the as-rolled condition with increasing rolling reduction.[13] Huang *et al.*[5–7,20] have extensively studied the recrystallization behavior of Al-Mn-Fe-Si alloys with different microchemistry states during isothermal and non-isothermal annealing, with special attention to the presence and evolution of the P-texture component. It is concluded that the P-component is affected by the microchemistry, the annealing temperature, and the heating rate. The strong P-texture is generally attributed to the effect of a significant Zener drag induced by dispersoids. However, although extensively studied, previous work is mainly qualitative while more quantitative studies on how concurrent precipitation affects the nucleation and growth behavior (in terms of nucleation density and growth rate) of different texture components (not only the P-component) are largely missing. Previous studies on Al-Mn alloys have documented that the strongest texture generally appears in the as-cast conditions which initially have high solute content (highest potential concurrent precipitation).[3,5,6] However, since the compared samples were based on the same alloy, it is unclear, besides high level of solutes, whether and to which extent possible micro-segregation affects recrystallization behavior.

The dominance of certain texture components is commonly explained by the oriented nucleation and rapid growth of grains with a 40 deg $\langle 111 \rangle$ orientation relationship to its surroundings. For example, in a commercial purity aluminum AA1050, it has been found that the growth of Cube,[21] P and ND-rotated cube components[22] is the fastest (consistent with the growth selection assumption mentioned above), the growth of the rolling components is the slowest,[21,22] while random components grow at an intermediate rate.[22] When recrystallization interacts with precipitates, it is found that Cube grains still grow faster than randomly oriented grains; however, ND-rotated cube and P grains grow even faster.[23,24] However, quantitative data are limited, and the growth rates of Cube, ND-rotated cube, and P orientations have not been compared so far in alloys where the effect of precipitation is weak.

On this background, the objective of the present work has been to investigate the nucleation and growth behavior of several typical recrystallization texture components in two cold rolled and annealed Al-Mn-Fe-Si alloys containing similar amounts of Mn in solid solution but different spatial distributions. An Al-Fe-Si alloy with limited potential for precipitation is used as reference material for comparing conditions which are differently affected by concurrent precipitation. The orientation-dependent evolution of grain structure is followed by electron backscattering diffraction (EBSD) imaging in a scanning electron microscope (SEM), while the precipitation behavior is also characterized in SEM. By correlating the orientation-dependent evolution of the grain structure and the precipitation behavior, the objective has been to document under which conditions the strong P- and ND-rotated cube components appear, to quantify the orientation-dependent nucleation and growth behavior in different conditions, and to possibly explain the differences documented. It is believed that

such quantitative data may provide valuable information which can be used to improve and further develop models for recrystallization texture evolution under various conditions.

II. EXPERIMENTAL

Aluminum alloys with three levels of Mn (labeled as C1, C2, and B, to be consistent with previous work on the same alloys[5–7]) and similar trace elements were fabricated in the same manner by Hydro aluminum. Their chemical compositions are listed in Table I. The B alloy is included as a reference, representing an alloy with very limited (concurrent) precipitation. Direct chill ingots with a diameter of 228 mm were produced, following standard casting practice. Samples for cold rolling were cut from the half radius location of the ingot. The average grain size of the as-cast alloys was ~100 μm, measured by the linear intercept procedure from optical micrographs. Various homogenization treatments prior to cold rolling were carried out for each alloy: (i) C1 corresponds to the as-cast state; (ii) C2 was homogenized at 873 K (600 °C) for 24 hours with a heating rate of 50 K/h, followed by water quenching; (iii) B was homogenized first at 873K (600 °C) for 24 hours with a heating rate of 50 K/h, then slowly cooled to 723 K (450 °C) (cooling took ~50 hours) and held for 34 hours, followed by water quenching. The alloys were rolled at room temperature from 30 mm down to 1.5 mm in thickness to achieve nominal reduction of 95 pct (corresponding to a strain of $\varepsilon = 3$), using lubricated rolls. The back annealing was performed in a salt bath. The normal and rolling direction (ND-RD) section of the samples was used for the microstructure and texture analysis in a FEG-SEM Zeiss Supra 55 and a Hitachi SU-6600, both equipped with an EBSD detector and TSL software. The sample surface was electro-polished in a 20 pct $HClO_4$ ethanol solution at 20 V and 253 K (-20 °C). The 2D number density per unit area of constituent particles was measured by backscattered electron (BSE) imaging of SEM. The 2D cumulative particle size distributions are plotted in Figure 1. To quantify the recrystallization nucleation behavior, recrystallization nuclei were defined to be (sub)-grains larger than 3μm in diameter and at least partially surrounded by high-angle boundaries, *i.e.*, similar to the definition used in Reference 22 The following orientations are studied in the present work (with their corresponding Euler angles): Cube (0, 0, 0), NDcube (20, 0, 0), and P (55, 45, 0). For C1, the P orientation is defined as (60, 45, 0) according to the ODF measurement. The maximum deviation angle is 10 deg. The definitions of NDcube and P used here are slightly different from those used in some literature; however, it is confirmed that these minor differences do not affect the analysis and conclusions. The scan area of each EBSD map was ~1 mm^2. Generally, two maps of EBSD scanning were used for the characterization of fully recrystallized samples, and three maps were used for partially recrystallized samples.

Table I. The Nominal Chemical Composition of Alloys (Weight Percent), Electrical Conductivity Prior to Cold Rolling (EC, MS/m), and the Area Fraction of Constituent Particles (Area Percent)

	Al	Mn	Fe	Si	EC	Area Percent
B	99.3	0.004	0.49	0.14	34.6	1.1
C1	98.9	0.39	0.53	0.15	24.1	2.3
C2	98.3	0.97	0.50	0.15	22.4	3.4
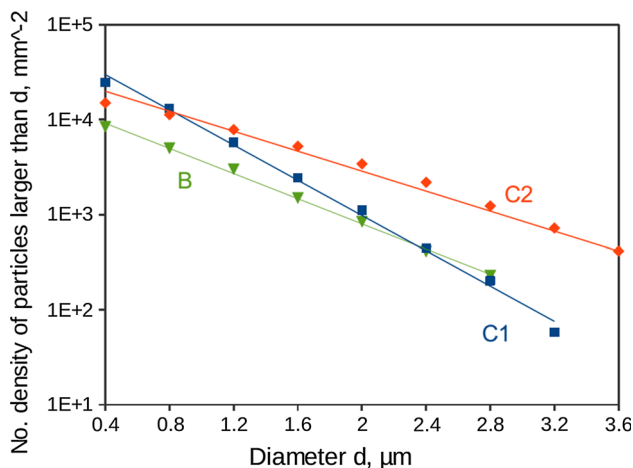
Fig. 1—Cumulative 2D size distributions of constituent particles in the different alloys after a rolling reduction of 95 pct.

III. RESULTS AND DISCUSSION

A. *Isothermal Annealing*

The Mn content in solid solution prior to cold rolling is estimated from the electrical conductivity (EC, MS/m), using the same method as in Reference 25:

$$1/EC = 0.0267 + 0.032 \text{ Fe pct} + 0.033 \text{ Mn pct} + 0.0068 \text{ Si pct} + 0.0021 \text{ Particle pct}, \quad [1]$$

where Fe pct, Mn pct, and Si pct are the weight percentages of the concentrations of these elements in solid solution. Particle pct is the volume fraction of particles, for which the area fraction measured by SEM is used as an approximation here. As suggested in Reference 25 the contributions from Fe and Si in solid solution are neglected due to their low concentrations. The estimated values of Mn pct in C1 and C2 are 0.30 and 0.33 wt pct, respectively, indicating similar Mn contents in solid solution in C1 and C2. Micro-segregations exist in C1 due to the as-cast structure. The B alloy shows a much higher EC value reflecting the very low concentration of solutes in this alloy. For the C2 material, Mn-containing dispersoids precipitate during heating;[26] however, most of them are dissolved during holding at 873 K (600 °C), and only a small amount remains after homogenization. The number density of dispersoids per unit area after homogenization was measured to be 1.2×10^4 mm^{-2}. At the same time, the constituent particles coarsened during homogenization, as indicated in Figure 1, where the C2 alloy is clearly seen to have a higher fraction of large particles than the C1 alloy. After cold rolling of 95 pct reduction, a typical β-fiber rolling texture is developed in these alloys. It has been shown that dispersoids can influence the texture development and grain subdivision during rolling.[27] However, the number density of dispersoids in C2 is small (in as-homogenized state), and hence, their effect is negligible.

The softening behavior of the C1 and C2 alloy and the corresponding evolution in electrical conductivity during annealing at selected temperatures are shown in Figure 2. Annealed at the same temperature, recrystallization kinetics of C2 is much faster than for C1. The electrical conductivity of C2 also seems to evolve faster than for C1 at the same temperature. For annealing at 573 K (300 °C), neither C1 nor C2 seems to experience any recrystallization, only extended recovery, and the general increasing trend of the EC curve indicates significant precipitation prior to recrystallization. At 773 K (500 °C), recrystallization finished within 5 seconds. All EC curves show a general increasing trend, however, with obvious changes in the rate where a distinct increased rate seems to occur simultaneously with the recrystallization reaction [as indicated by the corresponding drop in the hardness in Figures 2(a) and (c)], *i.e.,* for C2 during annealing at 623 K (350 °C) in the range of 100 to 10^4 seconds, for C2 at 673K (400°C) in the time range 5 to 100 seconds, and for C1 at 673 K (400 °C) between 10 and 1000 seconds. This observation indicates that significant precipitation (and dispersoid growth) occurred concurrently with recrystallization, and that the precipitation/growth kinetics was accelerated by the recrystallization reaction.

Precipitation prior to recrystallization and concurrent with recrystallization generally leads to a structure of coarse and strongly elongated grains, as exemplified for both the C2 and the C1 alloy annealed at 623 K (350 °C) (Figure 3), where the effect is clearly most pronounced for the C1 alloy. The RD-ND section of C1 in Figure 3(a) illustrates that the recrystallized grains are of pancake shape. Many small grains at boundaries and island grains are observed, which may be caused by grain boundaries of different mobilities.[1] The corresponding texture behavior is exemplified in Figures 4(a) through (d), where strong P and NDcube texture components appear after long-time annealing at low temperatures, *i.e.,* at 623 K (350 °C) [Figures 4(a) and (c)]. It is noted that the P-texture is clearly strongest for the C1 sample, accompanied by a weaker 45 deg ND-rotated cube component, while C2 has a weaker P-component accompanied with the more conventional 22.5 deg ND-rotated cube component. The 45 deg ND-rotated cube ({001} ⟨110⟩) orientation is a component of shear texture, which was often observed at the surface of heavily rolled aluminum.[4,28] When the alloys
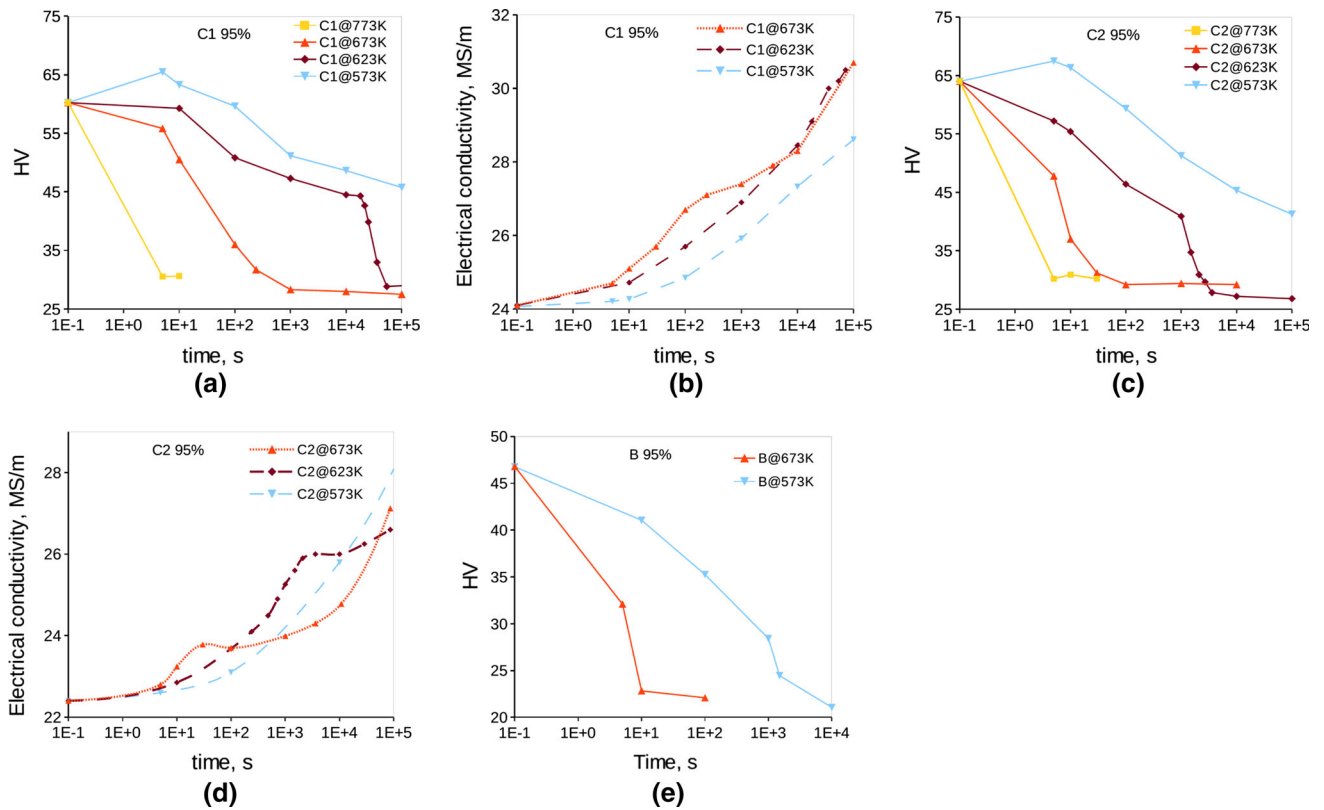
Fig. 2—The softening curves of alloy C1 (*a*), C2 (*c*), and B (*e*) indicated by hardness and the corresponding electrical conductivity curves (*b*, *d*). The measurements of as-rolled alloys are placed at 1E−1s.

were annealed at higher temperatures, the texture was usually weak and grain structure was close to equiaxed. For a more extensive study of the recrystallization structure and texture characteristics of these alloys, readers are referred to References 5, 6

The B alloy is a reference alloy for which the composition is similar to commercially pure aluminum. The similar concentrations of Fe and Si in the B alloy as that of C1 and C2 result in a comparable content of constituent particles, as shown in Figure 1. Most of solutes in B were depleted after the long-time homogenization and slow cooling, and hence very limited (concurrent) precipitation during annealing is expected in B. Thus, softening kinetics of B is much faster than for C1 and C2 (Figure 2). After annealing, the recrystallization texture of B is composed of a strong Cube and weak retained rolling components, as shown in Figures 4(e) and (f). However, as opposed to C1 and C2, no indications of the P-texture component were observed for this alloy.

B. *Nucleation of Recrystallization at Various Annealing Temperatures*

The texture evolution and final recrystallization texture are closely related to the nucleation and growth of recrystallized grains. Concurrent precipitation can affect both. In this section, the effect of concurrent precipitation on nucleation (early stage of growth) is investigated. The effect on growth will be discussed in

Section III–D. The number of recrystallized grains per unit area (mm^{-2}) was measured for the alloys annealed at various temperatures, which provides a measure of the nucleation density of recrystallization.

Figure 5 shows the number of grains per unit area in the different alloys annealed to full recrystallization at various annealing temperatures, *i.e.,* with various initial supersaturation and thus potential for precipitation and various extent of precipitation. The annealing time was selected according to the softening curves, just long enough to finish recrystallization, and to avoid further grain growth, because grain growth following primary recrystallization may change texture. The minimum annealing time was 5 seconds, which is for 773 K (500 °C). The results of C2 show two regimes in Figure 5(b). Above 673 K (400 °C), the number of grains per unit area is almost insensitive to annealing temperature. Below 673 K (400 °C), the grain density decreases as annealing temperature is reduced. The decrease regime corresponds to conditions of significant precipitation concurrent with or prior to recrystallization, which are indicated by the softening curves in Figure 2(b). In particular, it is noted that the number densities of special orientations such as P and NDcube grains decrease more slowly compared to other orientations, such as Cube and the overall number density, when annealed below 673 K (400 °C). A more detailed analysis of the recrystallization and precipitation behavior at 623 K (350 °C) is presented in the next section, as an example.
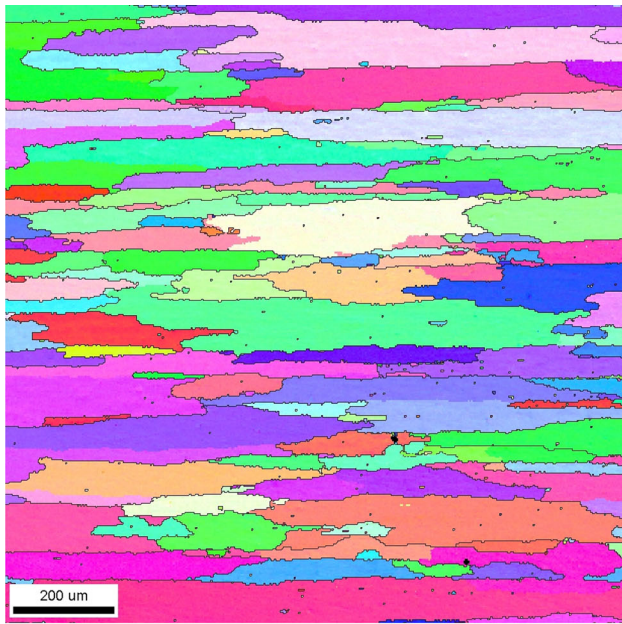
(a)
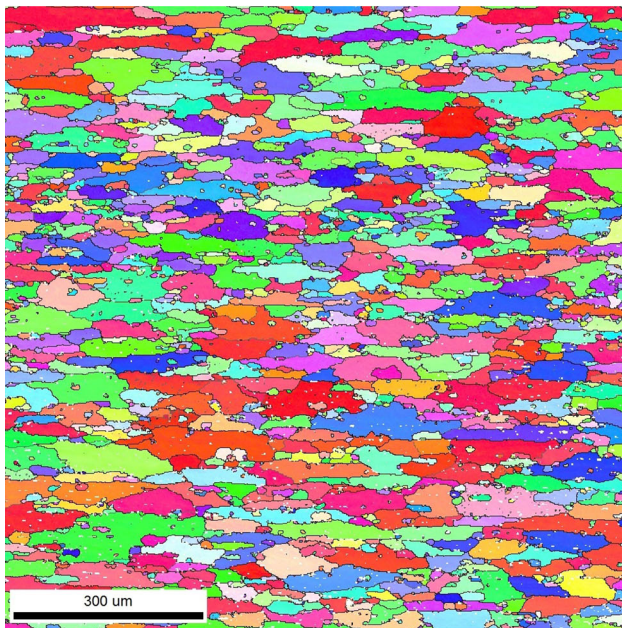
(b)

Fig. 3—Al-Mn-Fe-Si alloys cold rolled to 95 pct and annealed to full recrystallization at 623 K (350 °C): RD-ND section of C1 annealed for 10^5 s (a) and C2 annealed for 10^4 s (b) (vertical: ND).

The general trend of the C1 alloy is similar to that of C2, the difference being that the decrease regime is shifted to the slightly higher temperature of 698 K (425 °C) [Figure 5(a)]. Moreover, the difference between P and Cube orientations is even more obvious. The general observation is that the number density of P-oriented grains appears to be less affected by annealing temperature than the others. For C1 annealed at temperatures of 623 K and 648K (350 °C and 375 °C), the grains are coarse and very elongated [e.g., Figure 3(a)]. Thus, it was difficult to get a statistically
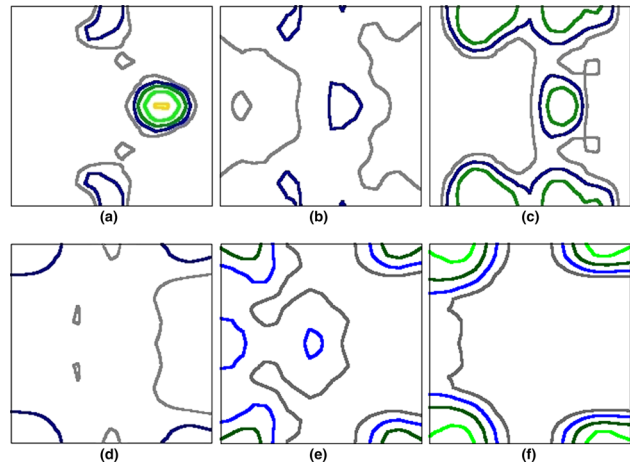
Fig. 4—The $\varphi_2 = 0$ section of ODF of 95 pct rolled C1, C2, and B annealed to full recrystallization: C1 at 623 K for 10^5 s [623 K (350 °C), a] and 723 K for 100 s [723 K (450 °C), b]; C2 at 623 K for 10^4 s [623 K (350 °C), c] and 723 K for 100 s [723 K (450 °C), d]; B at 573 K for 10^4 s [573 K (300 °C), e] and 673 K for 100 s [673 K (400 °C), f] (levels: 1 2 3.5 6 10).

reliable value for the number density of Cube grains. For the B alloy on the other hand for which no significant concurrent precipitation occurred (except a weak precipitation due to supersaturation of iron[29]), no evident effect of temperature on the nucleation density seemed to be present [Figure 5(c)]. It is noted from Figure 5 that the number density of NDcube is consistently higher than that of Cube. This is partly due to the deviation angle of 10 deg used in the present work. In the literature (e.g., Reference 24), 15 deg is commonly used for the Cube. Hence, part of the grains classified as NDcube in the present work would be classified as Cube according to the conventional definition in many other papers.

C. Simultaneous Recrystallization and Precipitation in Supersaturated Al-Mn-Fe-Si During Annealing at 623 K (350 °C)

As indicated by Figure 2(b), precipitation interacted strongly with recrystallization in C2 at 623 K (350 °C), and a more careful analysis by SEM-BSE is therefore presented in the following. Figure 6 shows the precipitation behavior in several different regions of the C2 specimen after 100 seconds at 623 K (350 °C). In Figures 6(a) and (b), precipitates have formed, mainly at sub-boundaries and around some coarse particles as well. However, the distribution of dispersoids is not uniform, as the density seems much higher in Figures 6(a) and (b) than in e.g., Figure 6(c). As exemplified in Figures 6(c) and (d), recrystallization has also started in this material after 100 seconds of annealing. As the annealing time increased, more precipitates were formed [Figure 7(a)], and recrystallized grains grew [Figure 7(b)]. As observed precipitates are mainly distributed along RD, which provides a stronger Zener drag in the ND than along RD,[16] and which thus gives recrystallized grains that are elongated in the rolling direction. It is noted that the dark vertical lines in
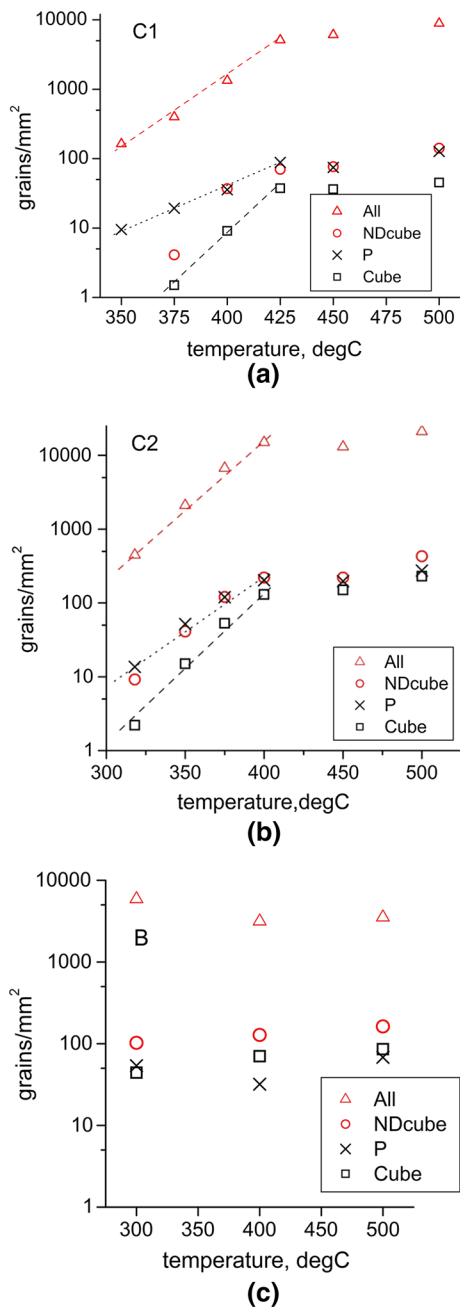
Fig. 5—Numbers of grains per unit area (mm^{-2}) in 95 pct rolled aluminum annealed at various temperatures to full recrystallization: (a) C1; (b) C2; (c) B.

Figures 6 and 7 are an artifact caused by the backscattered electron detector during slow scanning.

Dispersoids might coarsen during annealing, e.g., as suggested in the literature.[30] Coarsening of dispersoids reduces the Zener drag effect, and might allow new recrystallization grains to nucleate, i.e., subgrains to grow larger than the critical size for growth.[1] Thus, new nuclei of recrystallization might be formed continuously during annealing, i.e., time-dependent nucleation. Whether this applies for the present alloys is examined by the measurement of recrystallized grain density in partially recrystallized samples using EBSD. The scan

area of EBSD maps was ~1 mm^2, and 3 maps of EBSD scanning were used for each condition except that only one map was used for the 100 seconds condition and 4 maps used for the 1000 seconds condition. Only P- and Cube-oriented grains are considered for this analysis. The measured values of the grain number per unit area for each sample are plotted in Figure 8. The number per unit area increases with increasing annealing time.

Chan and Humphreys[31] measured recrystallized grain number per unit area of an Al-Si alloy containing fine particles during annealing for 0.5 to 72 hours. They found that the number density of grains per unit area was almost constant, and that the increased recrystallization fraction with annealing time was mainly attributed to grain growth rather than to forming new grains. It has also been reported that the number of recrystallized grains per unit volume was constant during annealing of commercially pure aluminum.[32] However, according to the data of sample C2 in Figure 8, the number of recrystallized grains per unit area appears to increase. An increase of the measured grain number per unit area could be caused by (1) actually more recrystallization nuclei formed (due to the coarsening of precipitates); or (2) the growth of recrystallized grains, which affects the cross section measurements. Generally, the number density per unit volume (N_V) can be estimated from the density per unit area (N_A) by Reference 33

$$N_V = N_A(kD)^{-1}, \qquad [2]$$

where D is the mean diameter of grains along the normal direction of the observation plane (TD in our case) and k is a constant of the order one. It is assumed here that the growth rates along TD and RD are the same, which is a reasonable assumption for the present samples. Then, the measured equivalent circle diameter is used as the value of D. The value of k is taken as unity since it does not influence the comparison. The calculated number per unit volume based on Eq. [2] is illustrated in Figure 9(a). As we see from the results in Figure 9, the evolution of recrystallized grain density per unit volume appears almost constant, indicating that formation of new recrystallization grains mainly occurs at the early stage of annealing, while no more new grains are formed later. Figure 9 also confirms that the number density of P grains per unit volume is clearly higher than that of Cube. The grain numbers per unit area from Figure 5 were also converted into numbers per unit volume. The qualitative trends of the different orientations are not changed. The difference in the average size of differently oriented grains (shown in Section III-D) evidently does not affect the comparison based on cross section measurements. As shown in Figure 9(b), the relative number of P-oriented grains as compared to the number of Cube grains increases as the annealing temperature is reduced below 673 K (400 °C).

D. Recrystallization Growth Influenced by Precipitation During Isothermal Annealing

The average grain diameters of selected orientations after full recrystallization of C1 and C2 are plotted in
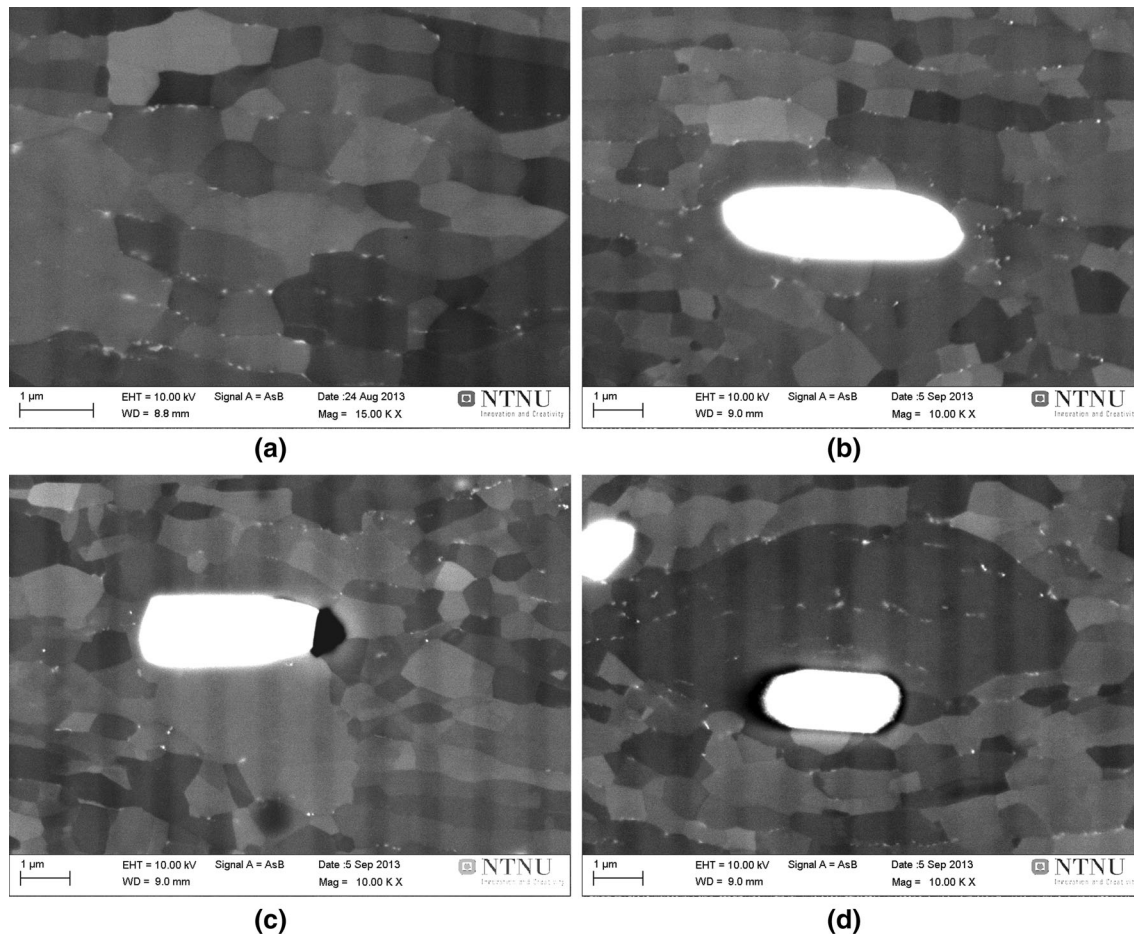
Fig. 6—Precipitation in different regions of the C2 alloy, cold rolled 95 pct and annealed at 623 K (350 °C) for 100 s: (*a*) subgrain structure away from particles, (*b*) particle surrounded by a unrecrystallized subgrain structure, (*c*, *d*) particles at which recrystallization has started and recrystallization grains grow into the surrounding sub-structure.

Figures 10(a) and (b), respectively. The general trend is that the grain size increases with decreasing annealing temperature, which is the result of the grain number density evolution as shown in Figure 5. Grain size also depends on their orientations. P, NDcube, and Cube grains are generally larger than the average size of all grains, indicating that these special orientations have experienced a growth advantage. When annealing at low temperatures, precipitation strongly interacts with recrystallization; the average grain sizes of P and NDcube are in most cases larger than that of Cube grains.

Figure 11(a) illustrates the average grain sizes of various orientations during isothermal annealing of C2 at 623 K (350 °C), based on the same data as in Figure 8. The corresponding evolution in microstructure and precipitation behavior has been discussed in Section III–C. The general trend is that when precipitation occurs concurrently with recrystallization, the average grain sizes of NDcube and P components are larger than that of Cube component, and they are larger than the average size of all orientations. Our results in Figure 11(a) are consistent with previous studies.[24] For comparison, the grain size in partially recrystallized B alloy was also measured, where Zener drag was almost absent. Figure 11(b) shows that Cube and NDcube have

the largest grain size, and the average size of P grains is a bit larger than the average size of all the grains. Comparison of the results in Figures 11(a) and (b) suggests that the relative growth advantage of Cube and P is significantly influenced by precipitation. Cube, NDcube, and P all have a general 40 deg ⟨111⟩ growth relation (or Σ7, literally 38 deg ⟨111⟩) with typical rolling texture components. Generally, grain boundaries with 40 deg ⟨111⟩ orientation relationship migrate faster than other boundaries,[1] and this is the basis for (micro)-growth selection mechanism for recrystallization textures in aluminum. However, the effect of precipitates on the growth of different orientations varies. Our results suggest that concurrent precipitation evidently suppresses the growth of the Cube component as compared to NDcube and P. A Zener drag effect caused by (concurrent) precipitation seems to affect the P orientation the least, while it significantly affects Cube-oriented grains.

It has been shown that if a typical rolling texture is numerically rotated by 38 deg about the 8 possible ⟨111⟩ axes, the resulting texture shows strong P and NDcube components, suggesting that these orientations have a higher fraction of a 38 deg ⟨111⟩ orientation relationship with the rolling texture components.[6,34] The 38 deg
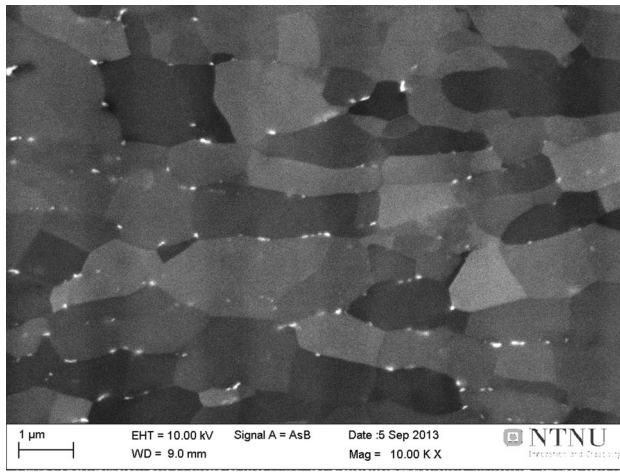
(a)
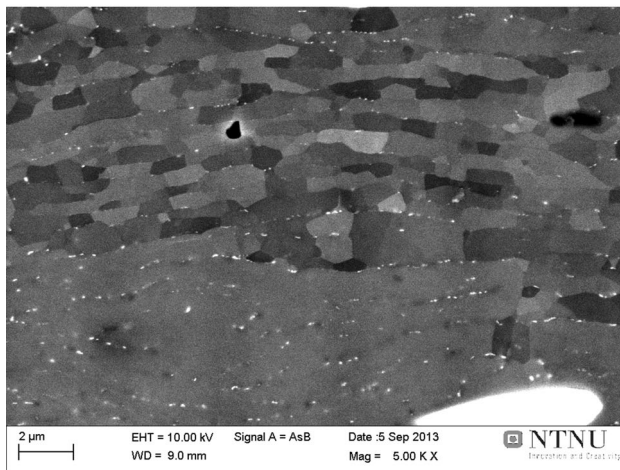
(b)

Fig. 7—SEM-BSE images of 95 pct rolled C2 alloy annealed at 623 K (350 °C) for 1000 s; showing sub-structure decorated by dispersoids (*a*), and partly recrystallized structures with dispersoids (*b*).
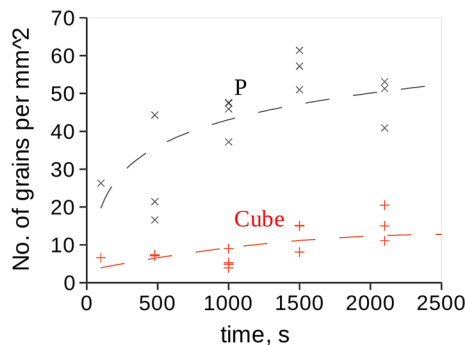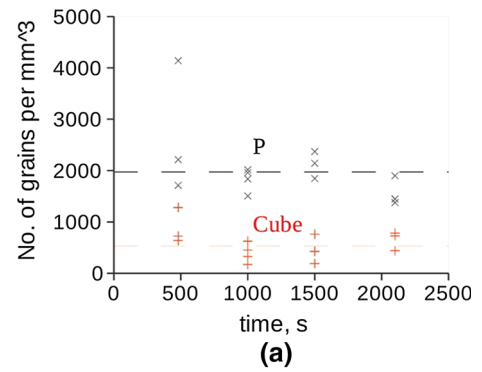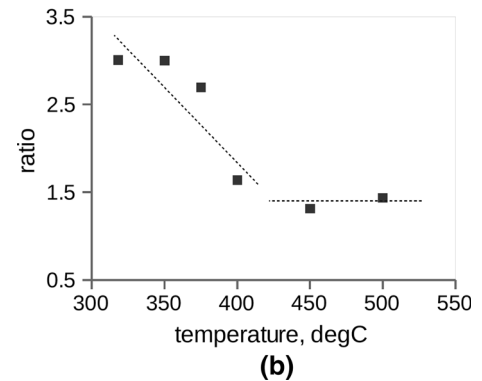

Fig. 8—The evolution of P- and Cube-oriented grains per mm^2 in C2 annealed at 623 K (350 °C).

$\langle 111 \rangle$ orientation relationship represents a $\Sigma 7$ special boundary (coincidence site lattice boundary; structurally more ordered than random high-angle grain boundaries), which has lower boundary energy and is supposed to be less affected by precipitation and solute drag effects. However, this particular orientation relationship

(a)

(b)

Fig. 9—(*a*) The evolution of grain number per mm^3 of P and Cube orientations in C2 annealed at 623 K (350 °C). All the calculated results from the measurements are plotted. (*b*) The ratio of grain number per mm^3 of P grains to Cube grains at various annealing temperatures.

is not the only important factor which influences the growth. If it is, P- and NDcube-oriented grains would always be larger than Cube-oriented grains, which is not consistent with our observations for sample B. Orientation pinning and local variations in stored energy are also important.[35] Thus, explaining a global growth advantage is difficult and not straightforward, as the nature of the grain boundary and local variations in stored energy between a recrystallized grain and the deformed matrix are expected to change all the time during growth.

E. *Orientation Preference of Recrystallization Texture*

In general, recrystallization textures can be explained by both a frequency and a size advantage of special orientations. The weak Cube texture after annealing with concurrent precipitation is not only due to its reduced growth rate but also due to its strongly suppressed nucleation. Recrystallization of P- and NDcube-oriented grains is, on the other hand, relatively less affected by concurrent precipitation than Cube- and other random-oriented grains (as indicated in Figure 5). Thus, P and NDcube become the dominant texture components at low annealing temperatures when concurrent precipitation is significant. Moreover, the effect of concurrent precipitation on the recrystallization texture (in terms of the P-texture intensity) is more pronounced in C1 than in C2 (Figure 4), and with a
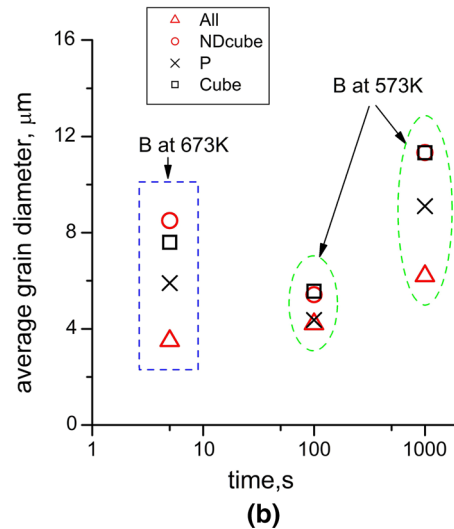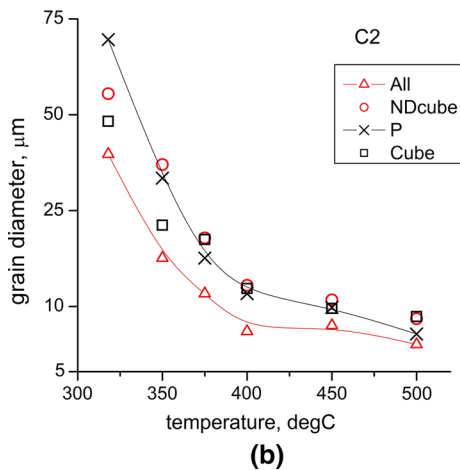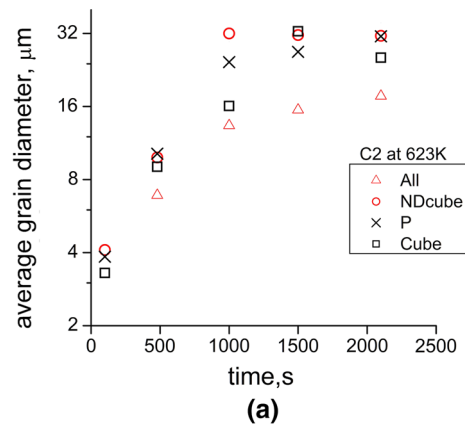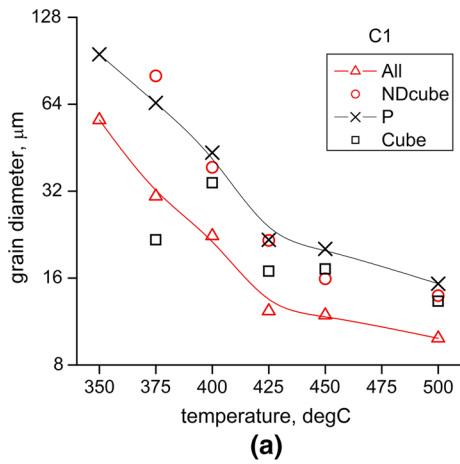
Fig. 10—The average grain sizes after full recrystallization in C1 (*a*) and C2 (*b*) at different annealing temperatures. The trend lines for P-oriented grains and for All grains are included.

Fig. 11—The average grain diameter as a function of annealing time: (*a*) C2 annealed at 623 K (350 °C), (*b*) B at 573 K (300 °C, for 100 and 1000 s) and 673 K (400 °C, for 5 s) (partially recrystallized).

clearly a stronger orientation preference in grain number density in C1 as well (Figure 5). C1 has similar solute content as C2 (after homogenization). However, since it contains micro-segregations due to its as-cast structure, precipitates concentrate at the periphery of original grain (and dendrite) boundaries. Figure 12 demonstrates the heterogeneous distribution of dispersoids precipitated during annealing in C1. Clusters of constituent particles are usually located near grain (and dendrite) boundaries, which could indicate the periphery of a grain/dendrite. The higher density of dispersoids retards recovery, leading to elongated subgrains, while recovered subgrains in regions with less dispersoids tend to be more equiaxed, as illustrated in Figure 12(b). The enhanced effect of concurrent precipitation in C1 clearly indicates that the nucleation of recrystallization at grain boundaries (*e.g.,* of Cube grains) is strongly suppressed by the heterogeneous precipitation, while special orientations such as P and NDcube, which are related to PSN, are less influenced, although their number densities are reduced as well.

A possible explanation for the orientation preference of recrystallization nucleation is that PSN may be less influenced by concurrent precipitation than recrystallization

occurred at grain boundaries due to the heterogeneous distribution of precipitation. PSN originates from pre-existing subgrains within the deformation zone, and it is suggested that potential nuclei with new high-angle grain boundaries (HAGBs) are formed by rapid sub-boundary migration during annealing due to the large orientation gradient and the high dislocation density within deformation zones.[1,8] It is well known that precipitation preferentially takes place at HAGBs rather than low angle boundaries or dislocations in Al-Mn alloys.[2] Thus, new HAGBs formed in the deformation zones around particles will initially have less precipitates per unit area than other original HAGBs (formed during solidification/deformation), and hence experience a lower Zener drag and a higher mobility. According to this reasoning, PSN is less affected by concurrent precipitation than recrystallization nucleation (and growth) at original grain boundaries. Cube grains on the other hand nucleate at transition bands or cube bands by strain-induced grain boundary migration, for both of which nucleation mainly relies on original HAGBs, and are thus more affected by precipitation.

It is generally accepted that PSN produces a more or less random spectrum of nucleus orientations, with a
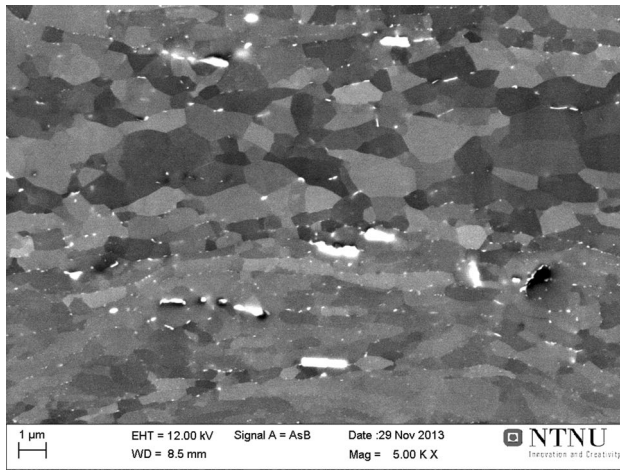
(a)
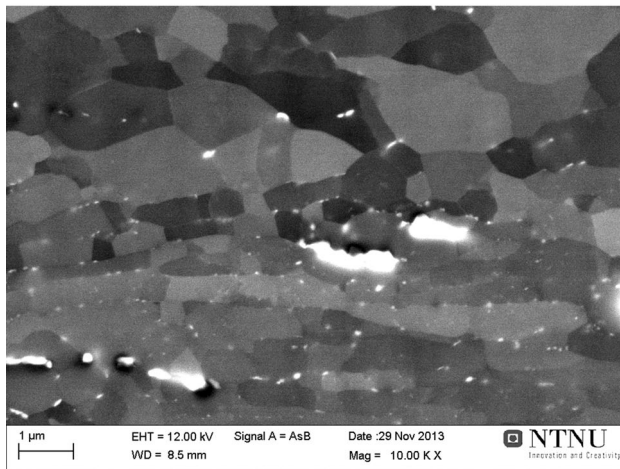
(b)

Fig. 12—95 pct rolled C1 annealed at 623 K (350 °C) for 10^4 s (*a*) and the same area in a larger magnification (*b*), showing heterogeneous distribution of dispersoids.

preference of P- and NDcube-oriented grains attributed to a 40 deg ⟨111⟩ growth selection, as suggested by Engler *et al.*[34] This particular growth selection seems to be enhanced in conditions of significant concurrent precipitation, explaining the dominance of the P- and NDcube components in these conditions. In this case, the growth of those "early nuclei" with other random orientations in general is strongly suppressed, and "only" P- and NDcube-oriented nuclei (which themselves are rare) seem able to further grow out of the deformation zones and into the surrounding matrix, becoming recrystallized grains. At this stage, a deformation structure with a few growing recrystallized grains, predominantly P- (and NDcube), surrounded by HAGBs will prevail, consistent with the observations in the literature.[12,36] The enhanced growth preference leads to coarse P- and NDcube-oriented grains, and these orientations finally dominate recrystallization texture. It is emphasized that our reasoning (possible explanation) is based on the experimental results available, although direct evidence of the proposed mechanisms by which the early stages of nucleation and recrystallization occur in these conditions is still mainly missing. It is evident that further experimental investigations are needed to clarify the actual behavior at the very early stages of nucleation/recrystallization in alloys and conditions where the P and NDcube become the predominant texture components. At the same time, it is acknowledged that this might be quite a challenge, as these are really rare events which might be difficult to identify and characterize.

IV. SUMMARY

When precipitation is absent or very weak, such as in the case of commercially pure aluminum, all nucleation sites are activated and their densities are almost insensitive to annealing temperature. The number fraction of P-oriented grains is very low, ~1 pct, and they do not have any growth advantage as is the case for Cube-oriented grains. Hence, P-texture does not usually appear due to its low grain number density and small grain size. In the absence of any Zener drag effect, Cube and ND-rotated Cube grow more rapidly than P and other orientations, leading to a recrystallization texture dominated by the Cube component.

In alloys with a significant potential for dispersoid precipitation (*i.e.,* high supersaturation of solutes) and when precipitation occurs concurrently with recrystallization, P and ND-rotated Cube become the main texture components. The effect is most pronounced at medium and lower annealing temperatures where precipitation in general is at its strongest. Concurrent precipitation generally suppresses the nucleation of recrystallization and retards growth. However, the effect varies for different orientations: significant for Cube, moderate for ND-rotated Cube, and the least for P-oriented grains. Micro-segregation around boundaries promotes local precipitation, enhancing the effect of concurrent precipitation on recrystallization nucleation. The strong P and ND-rotated texture components are attributed to nucleation and growth preferences, *i.e.,* both of which are less affected by concurrent precipitation as compared to other orientations. Firstly, the formation of P- and ND-rotated Cube, along with other early nuclei by particle-stimulated nucleation (PSN), is less influenced than the nucleation at grain boundaries due to the heterogeneous distribution of concurrent precipitation, which requires further investigations. Secondly, P- and ND-rotated Cube-oriented nuclei are more likely to grow out of the deformation zones and into the surrounding matrix due to a 40 deg ⟨111⟩ growth selection with the deformed matrix, and finally dominate the recrystallization texture.

REFERENCES

1. F.J. Humphreys and M. Hatherly: *Recrystallization and Related Annealing Phenomena*, Elsevier, Amsterdam, 2004.
2. M. Somerday and F.J. Humphreys: *Mater. Sci. Technol.*, 2003, vol. 19, pp. 20–29.
3. S. Tangen, K. Sjølstad, T. Furu, and E. Nes: *Metall. Mater. Trans. A*, 2010, vol. 41A, pp. 2970–83, DOI:10.1007/s11661-010-0265-8.
4. S. Benum and E. Nes: *Acta Mater.*, 1997, vol. 45, pp. 4593–602, DOI:10.1016/S1359-6454(97)00157-2.
5. K. Huang, N. Wang, Y. Li, and K. Marthinsen: *Mater. Sci. Eng. A*, 2014, vol. 601, pp. 86–96, DOI:10.1016/j.msea.2014.02.037.
6. K. Huang, O. Engler, Y.J. Li, and K. Marthinsen: *Mater. Sci. Eng. A*, 2015, vol. 628, pp. 216–29, DOI:10.1016/j.msea.2015.01.064.
7. K. Huang, Q. Zhao, Y. Li, and K. Marthinsen: *J. Mater. Process. Technol.*, 2015, vol. 221, pp. 87–99, DOI:10.1016/j.jmatpro-tec.2015.02.016.
8. F.J. Humphreys: *Acta Metall.*, 1977, vol. 25, pp. 1323–44, DOI:10.1016/0001-6160(77)90109-2.
9. Y. Zhang, D. Juul Jensen, Y. Zhang, F. Lin, Z. Zhang, and Q. Liu: *Scr Mater*, 2012, vol. 67, pp. 320–23, DOI:10.1016/j.scripta-mat.2012.05.006.
10. H.E. Vatne, O. Engler, and E. Nes: *Mater. Sci. Technol.*, 1997, vol. 13, pp. 93–102, DOI:10.1179/mst.1997.13.2.93.
11. O. Engler, H.E. Vatne, and E. Nes: *Mater. Sci. Eng. A*, 1996, vol. 205, pp. 187–98, DOI:10.1016/0921-5093(95)09879-8.
12. C. Schäfer, J. Song, and G. Gottstein: *Acta Mater.*, 2009, vol. 57, pp. 1026–34, DOI:10.1016/j.actamat.2008.10.052.
13. C. Schäfer and G. Gottstein: *Int. J. Mater. Res.*, 2011, vol. 102, pp. 1106–14, DOI:10.3139/146.110567.
14. J.J. Sidor, R.H. Petrov, and L.A.I. Kestens: *Acta Mater.*, 2011, vol. 59, pp. 5735–48, DOI:10.1016/j.actamat.2011.05.050.
15. J.J. Sidor, K. Decroos, R.H. Petrov, and L.A.I. Kestens: *Int. J. Plast*, 2015, vol. 66, pp. 119–37, DOI:10.1016/j.ijplas.2014.08.009.
16. E. Nes, N. Ryum, and O. Hunderi: *Acta Metall.*, 1985, vol. 33, pp. 11–22, DOI:10.1016/0001-6160(85)90214-7.
17. W.C. Liu and J.G. Morris: *Scr Mater*, 2007, vol. 56 (3), pp. 217–20, DOI:10.1016/j.scriptamat.2006.10.011.
18. W.C. Liu, H. Yuan, and M.J. Huang: *Metall. Mater. Trans. A*, 2009, vol. 40A, pp. 2794–97, DOI:10.1007/s11661-009-9998-7.
19. Q. Zeng, X. Wen, and T. Zhai: *Metall. Mater. Trans. A*, 2009, vol. 40A (10), pp. 2488–97, DOI:10.1007/s11661-009-9942-x.
20. K. Huang, Y.J. Li, and K. Marthinsen: *J. Mater. Sci.*, 2015, vol. 50 (14), pp. 5091–5103, DOI:10.1007/s10853-015-9063-4.
21. D. Juul Jensen: *Acta Metall. Mater.*, 1995, vol. 43, pp. 4117–29, DOI:10.1016/0956-7151(95)00111-8.
22. O.V. Mishin, D. Juul Jensen, and N. Hansen: *Metall. Mater. Trans. A*, 2010, vol. 41A, pp. 2936–48, DOI:10.1007/s11661-010-0291-6.
23. O. Engler: *Mater. Sci. Technol.*, 1996, vol. 12, pp. 859–72, DOI:10.1179/mst.1996.12.10.859.
24. O. Daaland and E. Nes: *Acta Mater.*, 1996, vol. 44, pp. 1413–35, DOI:10.1016/1359-6454(95)00290-1.
25. Q. Zhao, B. Holmedal, and Y. Li: *Philos. Mag.*, 2013, vol. 93 (22), pp. 2995–3011, DOI:10.1080/14786435.2013.794315.
26. Y.J. Li and L. Arnberg: *Acta Mater.*, 2003, vol. 51 (12), pp. 3415–3428, DOI:10.1016/S1359-6454(03)00160-5.
27. Q. Zhao and B. Holmedal: *Trans. Nonferrous Met. Soc. China*, 2014, vol. 24, pp. 2072–78, DOI:10.1016/S1003-6326(14)63314-8.
28. W. Truszkowski, J. Krol, and B. Major: *Metall. Trans. A*, 1982, vol. 13A, pp. 665–69, DOI:10.1007/BF02644432.
29. S. Bunkholt: PhD Thesis, Norwegian University of Science and Technology, Trondheim, 2013.
30. N. Wang, J.E. Flatøy, Y. Li, and K. Marthinsen: *ICAA13: 13th International Conference on Aluminum Alloys*, Wiley, 2012, pp. 1837–42, DOI:10.1002/9781118495292.ch275.
31. H.M. Chan and F.J. Humphreys: *Acta Metall.*, 1984, vol. 32, pp. 235–43, DOI:10.1016/0001-6160(84)90052-X.
32. D. Juul Jensen, N. Hansen, and F.J. Humphreys: *Acta Metall*, 1985, vol. 33, pp. 2155–62, DOI:10.1016/0001-6160(85)90176-2.
33. F.N. Rhines and R.T. DeHoff, eds.: *Quantitative Microscopy*, McGraw-Hill, New York, 1968.
34. O. Engler, P. Yang, and X.W. Kong: *Acta Mater.*, 1996, vol. 44, pp. 3349–69, DOI:10.1016/1359-6454(95)00416-5.
35. G.H. Fan, Y.B. Zhang, J.H. Driver, and D. Juul Jensen: *Scr Mater.*, 2014, vols. 72–73, pp. 9–12, DOI:10.1016/j.scriptamat.2013.09.031.
36. O.V. Mishin, A. Godfrey, D. Juul Jensen, and N. Hansen: *Acta Mater.*, 2013, vol. 61, pp. 5354–64, DOI:10.1016/j.actamat.2013.05.024.